The International Journal of Advanced Manufacturing Technology (2019) 103:77–89
https://doi.org/10.1007/s00170-019-03546-z

ORIGINAL ARTICLE

Adaptive speed control for waterjet milling in pocket corners

Van Hung Bui[1] · Patrick Gilles[1] · Tarek Sultan[1] · Guillaume Cohen[1] · Walter Rubio[1]

Received: 27 July 2018 / Accepted: 4 March 2019 / Published online: 15 March 2019

Abstract
Milling thin titanium alloy workpieces using conventional manufacturing processes is a delicate operation. During machining, the cutting forces can deform the part, while resulting compressive stresses could actually enhance its mechanical properties. Nevertheless, when parts are both large in size and thin, deformation generated by machining will be incompatible with the geometrical specifications. From this perspective, abrasive waterjet milling offers a suitable alternative solution. Numerous works present the results relating to the depths milled, the surface characteristics and machining strategies when milling pockets. Such studies show that the change of direction when milling closed pockets generates defects arising from the distribution of the jet's energy over the milled surface or the kinematics of the machine. When a pocket corner radius is imposed, changes of direction are made following circular arcs with a radius lower than the specified one. In the present paper, an analysis of the width milled during successive circular trajectories is presented and a predictive model for the depth is adopted. This model is then used to propose a milling method that allows both the imposed radius and tolerance on the pocket depth to be respected.

Keywords Machining · Abrasive waterjet · Milling strategy · Titanium alloy · Ti6Al4V

1 Literature review

Titanium alloys have excellent mechanical properties, and one of the most commonly used is the Ti6Al4V alloy. This grade is mainly composed of titanium, aluminium (6%), vanadium (4%), and other constituents such as carbon (0.08%), iron (0.25%), oxygen (0.13%), nitrogen (0.05%) and hydrogen (0.012%). The main properties of this alloy are high tensile strength (860 MPa), high yield strength (800 MPa) and an elongation of more than 10%. It is therefore difficult to machine using conventional turning and milling methods due to its high strength and galling tendency. During such machining, the cutting forces can become high and cause deformations in the workpiece or significant excess heating. In both cases, the finished workpiece's geometry will show deviations outside specifications. This situation is exacerbated when the workpieces are part of an aerostructure that must be resistant, of large dimensions and lightweight. Achievement of these last two properties often requires the use of thin walls that are difficult to machine as they are extremely deformable and sensitive to vibrations.

Other material removal solutions have been studied to overcome the difficulty of milling such parts. Among them, abrasive waterjet milling is a highly interesting alternative solution as it uses natural components (water and abrasive) and only generates low cutting forces. It thus limits deformation of the workpiece and resolves some production waste recycling issues. This process has thus been widely studied to machine open or closed pockets [1–3]. In the case of closed pockets, the various strategies necessarily generate changes of direction during machining. In their study, Goutham et al. [4] consider rectangular pockets and changes of direction at 90°. This study shows that the changes of direction lead locally to defects in the pocket depth (Fig. 1). When the jet slows down

✉ Van Hung Bui
van-hung.bui@univ-tlse3.fr

Patrick Gilles
patrick.gilles@insa-toulouse.fr

Tarek Sultan
tarek.sultan@insa-toulouse.fr

Guillaume Cohen
guillaume.cohen@univ-tlse3.fr

Walter Rubio
walter.rubio@univ-tlse3.fr

[1] Institut Clément Ader (ICA), CNRS-INSA-ISAE-Mines Albi-UPS, Université de Toulouse, France, 3, rue Caroline Aigle, 31400 Toulouse, France

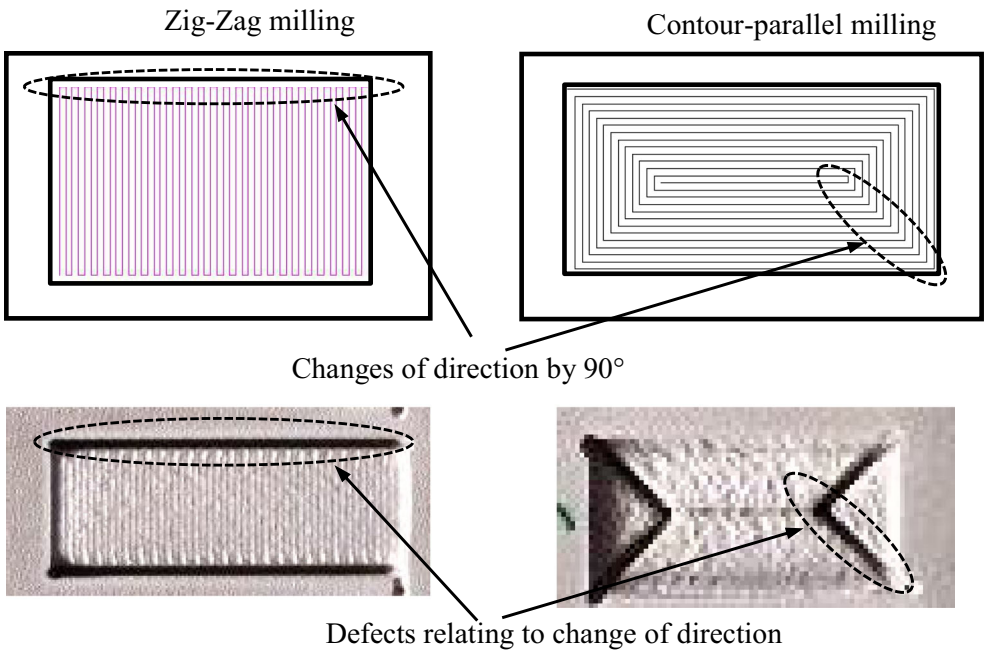

Fig. 1 Changes in milling direction by 90° and corresponding defects [4]

and then stops to change feed direction, the workpiece's exposure time increases and the depth machined increases.

In their works, Alberdi et al. [1] presented the milling of triangular pockets (Fig. 2) based on two strategies using changes of different directions by 90°. One pocket produced in parallel contours was machined moving, in one instance, from the interior to the exterior and in the other instance moving from the exterior to the interior. All the pockets showed irregularities on the bottom depth (Fig. 2). These irregularities appeared in the zones where changes of direction were made.

In the same study, an analysis of the defects generated on change of direction is presented and it is stated that the variation in the distance between two adjacent trajectories is the origin of the observed defect. When the trajectories are parallel, the distance between the point situated under the jet and the point closest to the already milled surface is constant. This distance is

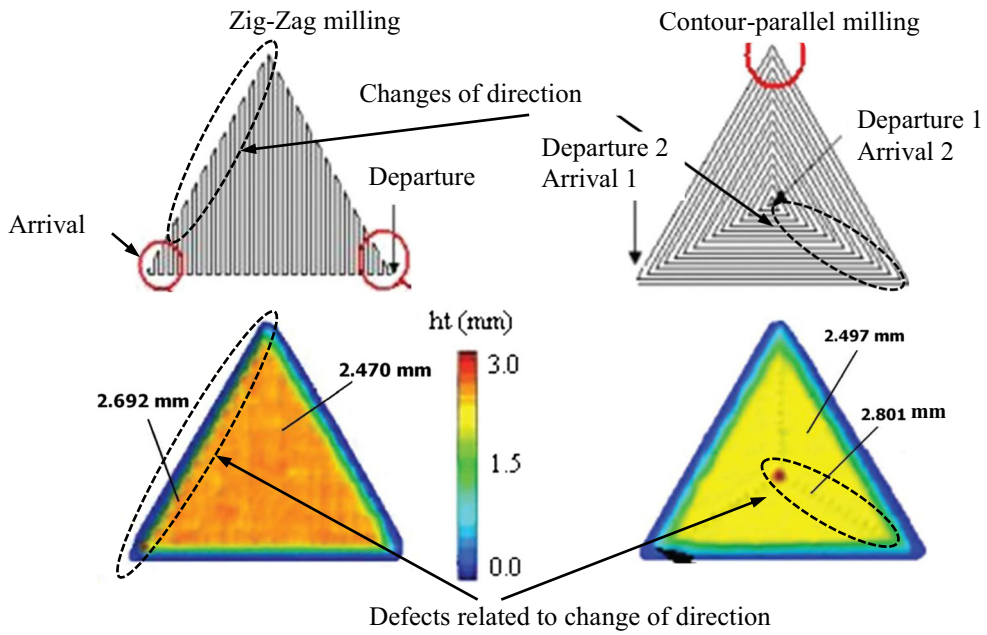

Fig. 2 Changes of direction for triangular pockets [1]

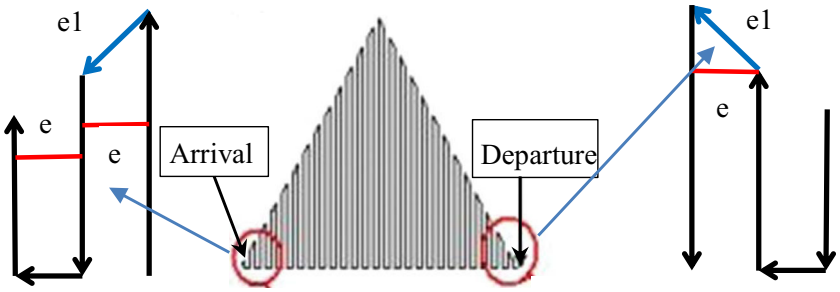

Fig. 3 Distances on changes of direction

greater when there is a change of direction (Fig. 3), and this generates a difference in depth. The variation in distance between two successive passes is thus one of the causes of the variation in depth milled.

2 Change of direction

2.1 Depth model for milled pockets

To predict the depth of the milled pockets, modelling of their shape is required. Different approaches have been used to determine the influence of machining parameters on the milled surface. These approaches are based on experiments [1–7], on an advanced computational method [8], on design of experiment [9], on analysis of the material removal mechanism [10], on analysis of the surface roughness [11] or on a CFD method [12]. It is also possible to consider an elementary profile [12–15] to model it [12, 14] and calculate the equation for a pocket bottom profile by considering an offset between each pass [9, 15].

The setting parameters are not modifiable during milling: They are pressure (*P*), a grade of abrasive particle, the abrasive flow rate (ma) and the standoff distance (*SOD*). The control parameters are those that can be controlled by the NC program during machining. Considering an elementary pass, the only controlled parameter is the traverse speed (*Vf*).

Among proposed models, the model based on an exponential function is effective in modelling an elementary pass. This elementary pass is generated by moving the jet in a straight line over a machined surface of the workpiece (Fig. 4a). Several studies on metallic materials [1, 7, 15] have confirmed that the profile of an elementary pass can be represented using the Gaussian profile (Eq. 1).

$$y(x) = -H \times e^{\left(-\frac{x^2}{B^2}\right)} \tag{1}$$

This Gaussian profile (Fig. 4b) is characterised by the maximum depth H and the width factor B [15]. They are established using a power function (Eq. 2). The width of the profile is estimated by the interval of $[-2xB; 2xB]$ and contains all the points of the profile curve where $y(x) \leq -0.01xH$. This consideration excludes cases of particle impacting without removing material.

$$H(Vf) = Ho \times Vf^{Hv} \quad \text{and} \quad B(Vf) = Bo \times Vf^{Bv} \tag{2}$$

In this expression, *Ho*, *Hv*, *Bo* and *Bv* are experimental coefficients calculated by the least squares method. Traverse

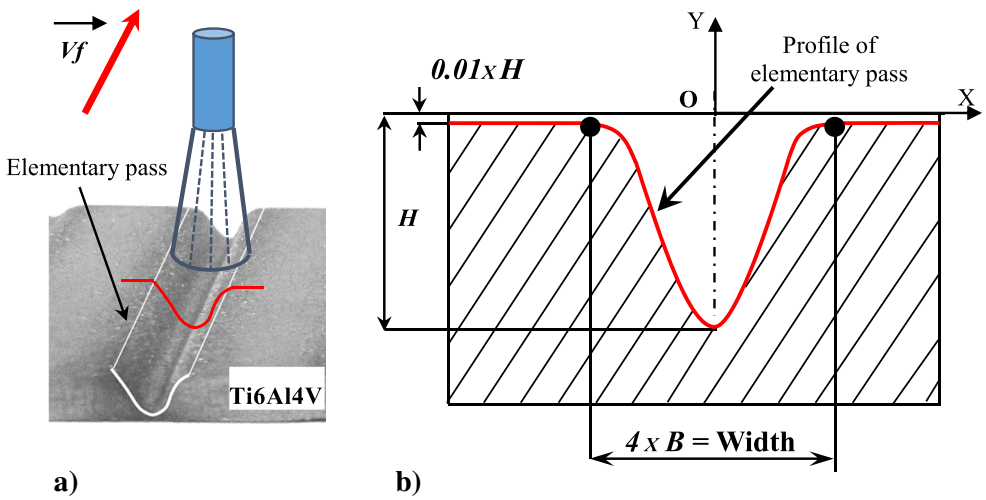

Fig. 4 Modelling the Gaussian profile

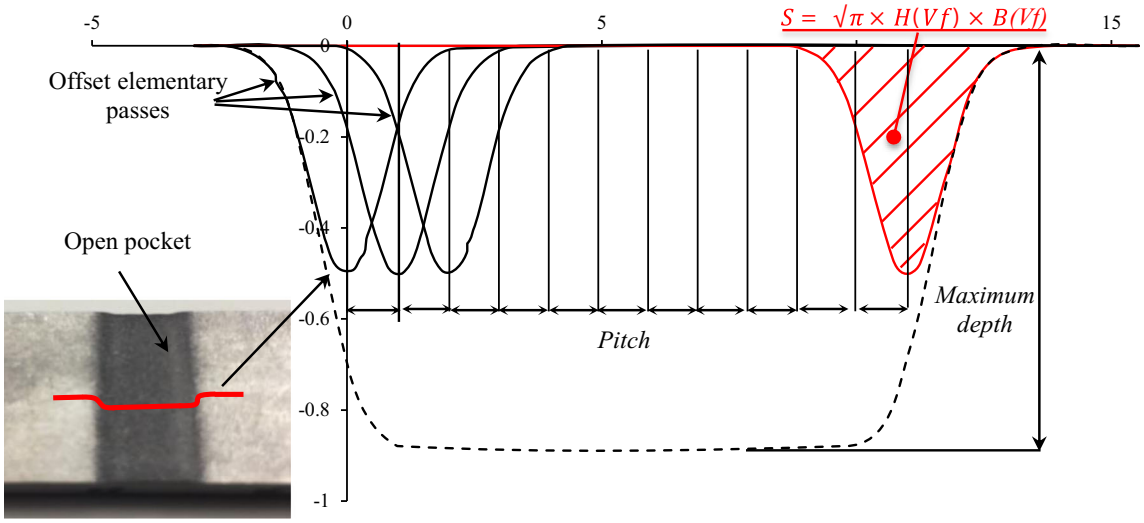

Fig. 5 Superposition of elementary passes

speed Vf is expressed in millimetres per minute and $H(Vf)$ and $B(Vf)$ are obtained in millimetres.

As an elementary profile is characterised by the equation (Eq. 1), it is possible to determine the cross section profile of an open pocket bottom as being the sum of n elementary passes (Fig. 5) with an offset distance named $Pitch$. According to Eq. 1, Eq. 3 expresses the superposition of n offset elementary passes for a given $Pitch$:

$$Y(x) = Ke \times \sum_{i=0}^{n} \left[H(Vf) \times e^{\left(-\frac{(x - i \times Pitch)^2}{B(Vf)^2} \right)} \right] \tag{3}$$

In this equation, the coefficient Ke allows an additional erosion that appears when a succession of elementary passes is performed to be taken into account. This erosion arises from the action produced by a given pass on the surface generated by the previous passes. Indeed, the main material removal mechanism [16–18] identified suggests that a particle does not fragment on impact and that it is driven by a plane movement. Hence, it generates an additional erosion (a second effect of impacting particles) on the surface that has already been milled.

Once the maximum depth has been reached, it can be specified according to Eq. 4 [15].

$$Maximum\ depth = Ke \times \frac{\sqrt{\pi} \times H(Vf) \times B(Vf)}{Pitch} \tag{4}$$

It should be noted that it is possible to modify the jet's impact angle by tilting the cutting head. In their work, Hlavac et al. [19] use the tilting angle in order to reduce the product shape distortion in water jet cutting. In this study, only an impact angle of 90° will be considered, while a variable angle will be studied in a forthcoming work.

2.2 Direction change strategies

The issue studied in the present paper concerns milling of closed pockets for which changes of direction by 90° are needed. On a change of direction without circular arc (Fig. 6a), the machine has to decelerate (Fig. 6c) down to zero speed, change direction and accelerate to again reach the specified traverse speed. During the deceleration and acceleration phase, the jet remains longer on the same location than during a continuous trajectory at constant speed. A greater depth thus inevitably emerges (Fig. 6a). To avoid this problem, the direction can be changed using circular arc trajectories (Fig. 6b).

Several solutions are possible to change direction using circular arc trajectories:

- Concentric arcs (Fig. 6d) allow the distance between two consecutive passes to be retained. The quantity of energy of the jet will then be distributed over the same milled surface quantity, and the depth will remain constant. However, the pocket corner radius will depend on the number of passes needed to produce the pocket and cannot therefore respect a specification.
- Constant radius arcs (Fig. 6e) allow a set radius to be maintained. The distance between two consecutive arcs will not be constant, and the energy distribution of the jet over a surface quantity will depend on the jet's position. This surface quantity will be maximal when the jet is in the middle of the circular arc. The depth machined will thus be reduced in the pocket corner that will then show a bump (Fig. 6g). Failing correction, this pocket corner will resemble a speed bump.

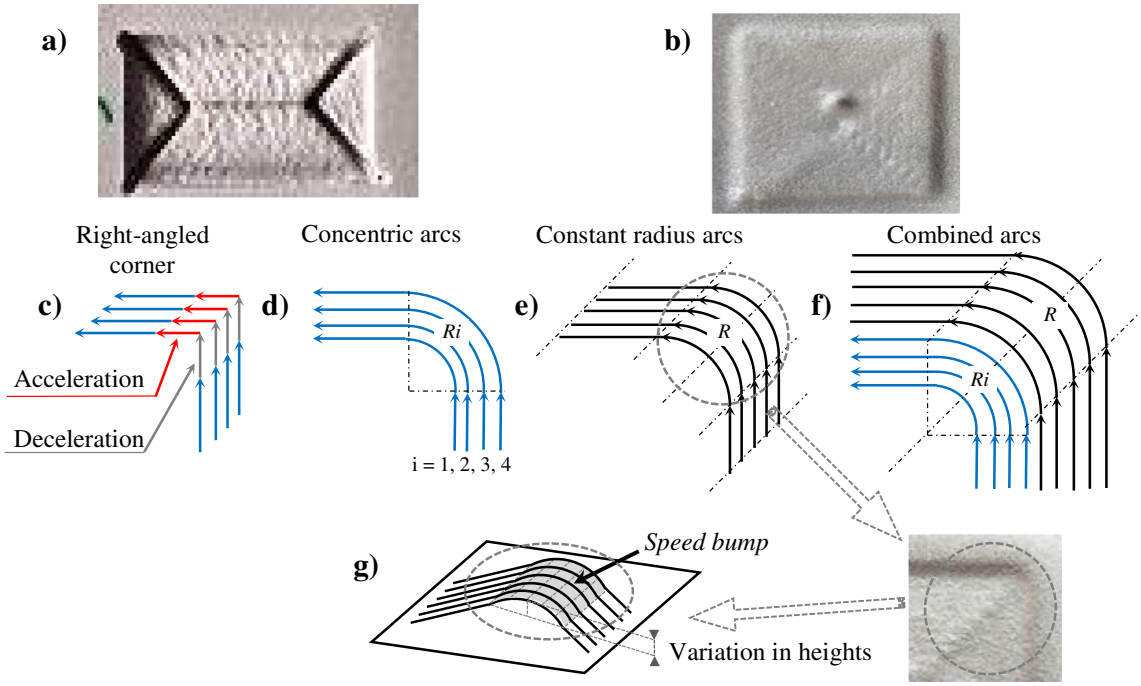

Fig. 6 Different changes of direction

– A combination of the previous solutions (Fig. 6f) allows the pocket corner radius to be controlled. This solution uses the small radius needed in the centre of the pocket and limits its value on the outer radius specified R once it has been reached. If no correction is applied, the pockets obtained will have a constant depth as long as the radii remain concentric but will show speed bumps when the radius remains constant.

2.3 Change of direction at constant radius

2.3.1 Identification of three distinct areas

When the arcs have a constant radius, the distance between two consecutive passes will vary according to the point considered on the trajectory. This distance is calculated as the length of the perpendicular to the mid-line between two passes. Geometrically, evolution of the distance has a mathematical relationship with initial pitch, $Pitch_{init}$. In the present work, the initial pitch $Pitch_{init}$ will be quite small in relation to the radius R of the pocket corner ($Pitch_{init} \ll R$).

Figure 7 illustrates the change in distance of two adjacent toolpaths, i.e. outer toolpath (A_1, B_1, D_1, E_1) and inner toolpath (A_2, B_2, D_2, E_2) at a corner of a milled pocket with constant radius R. Three areas need to be defined for an angle smaller than 45°, and a different calculation has to be performed of the distance for each of them:

– *Area 1*: the inner path is a circular arc, and the mid-line and the outer path are line segments. This area corresponds to an angle sector θ_1. Angles in this sector are negative.
– *Area 2*: the inner path and the mid-line are circular arcs, the outer path is a straight line. This area corresponds to an angle sector θ_2.
– *Area 3*: the inner path, the mid-line, and the outer path are circular arcs. This area is limited at an angle of 45° on the corner with the angle sector θ_3.

For the rest of the trajectory, the calculation is performed similarly using the symmetry.

2.3.2 Evaluation of the distance in three different areas

Considering the origin (O_{C2}, X, Y), the equation of the circle corresponding to the inner toolpath (C_2) can be written (Eq. 5):

$$(C2) : x^2 + y^2 = R^2 \tag{5}$$

Considering the same origin (O_{C2}, X, Y), the equation of the circle corresponding to the outer toolpath (C_1) and the

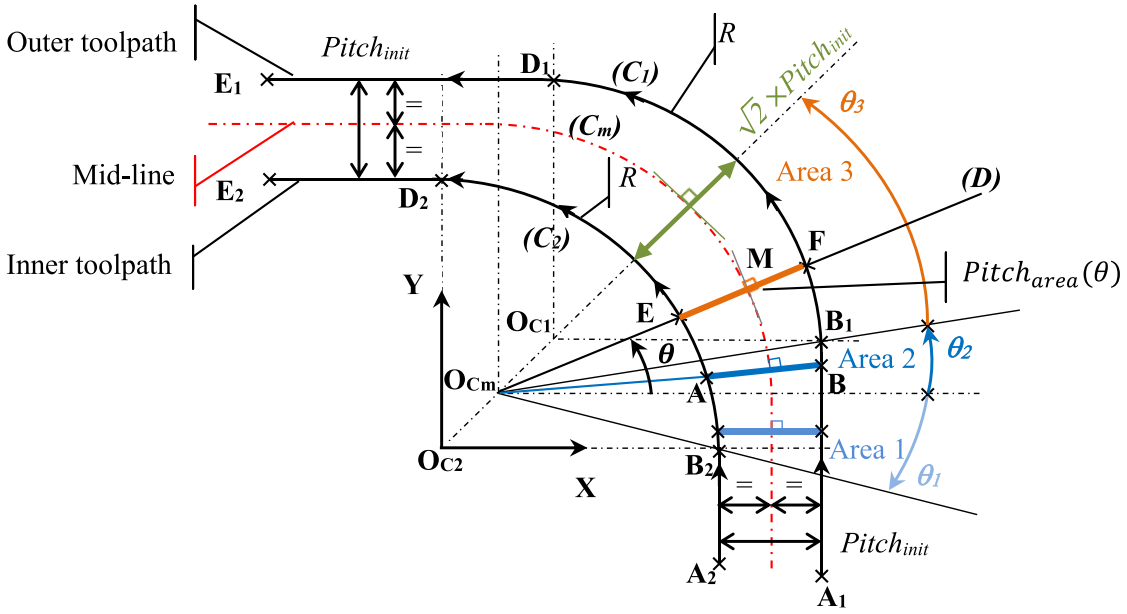

Fig. 7 Changes of direction at constant radius

equation of the circle corresponding to the mid-line (C_m) can be written (Eq. 6):

$$\begin{aligned}(\mathrm{C1}) &: (x-x_{o1})^2 + (y-y_{o1})^2 = R^2 \\ (Cm) &: (x-x_o m)^2 + (y-y_o m)^2 = R^2\end{aligned} \tag{6}$$

From Fig. 7, the coordinates of centre points O_{C1} and O_{Cm} belonging to (C_1) and respectively to (C_m) can be expressed (Eq. 7):

$$\begin{aligned}(\mathrm{OC1}) &: x_{o1} = y_{o1} = Pitch_{init} \\ (O_{Cm}) &: x_{om} = y_{om} = \frac{Pitch_{init}}{2}\end{aligned} \tag{7}$$

In addition, the vertical line (A_1B_1) is established (Eq. 8):

$$(A1\ B1) : x = R + Pitch_{init} \tag{8}$$

The normal to the circular arc (C_m) at each point M is defined by the straight line (D) passing through the point O_{Cm} (x_{om}, y_{om}) and its equation can be written according to θ (Eq. 9):

$$(D) : y = \tan(\theta) \times \left(x - \frac{Pitch_{init}}{2}\right) + \frac{Pitch_{init}}{2} \qquad \text{for } 0 \le \theta \le \frac{\pi}{4} \tag{9}$$

Using Eqs. 5 to 9, the distances $Pitch_{area}(\theta)$, for the three areas 1, 2 and 3, can be evaluated. Results are shown in Table 1. The detailed calculation can be found in Appendix.

These expressions can be simplified when the initial pitch is very small compared with the corner radius ($Pitch_{init} \ll R$). Corresponding results are presented in Table 2.

From Table 2, it can be established that when the initial pitch is very small compared with the corner radius ($Pitch_{init} \ll R$), the distance between two consecutive passes does not depend on the magnitude of the corner radius R. A computation of the distance along the middle line using the symmetry in relation to the middle of the corner is performed. A representation is given (Fig. 8a) for different values of the

Table 1 Distance in three areas

	Angle (θ)	$Pitch_{area}(\theta)$
Area 1	$\theta \in \left[\mathrm{atan}\left(\frac{-Pitch_{init}/2}{R-Pitch_{init}/2}\right); 0\right]$	$R + Pitch_{init} - \sqrt{R^2 - [(R-Pitch_{init}/2)\tan\theta + Pitch_{init}/2]^2}$
Area 2	$\theta \in \left]0; \mathrm{atan}\left(\frac{Pitch_{init}/2}{R+Pitch_{init}/2}\right)\right]$	$\frac{R+Pitch_{init}/2}{\cos\theta} + \frac{\sqrt{2}}{2}Pitch_{init}\cos\left(\frac{\pi}{4}-\theta\right) - \frac{1}{2}\sqrt{4R^2 - 2Pitch_{init}{}^2\sin^2\left(\frac{\pi}{4}-\theta\right)}$
Area 3	$\theta \in \left]\mathrm{atan}\left(\frac{Pitch_{init}/2}{R+Pitch_{init}/2}\right); \frac{\pi}{4}\right]$	$\sqrt{2}Pitch_{init}.\cos\left(\frac{\pi}{4}-\theta\right)$

Table 2 Distance in three areas considering $Pitch_{init} \ll R$

	Angle (θ)	$Pitch_{area}(\theta)$
Area 1	$\theta \cong 0$	$\cong Pitch_{init}$
Area 2	$\theta \in \left]0; \operatorname{atan}\left(\frac{Pitch_{init}/2}{R+Pitch_{init}/2}\right)\right]$	$\cong \frac{Pitch_{init}}{2}\left(1+\sqrt{2}\cos\left(\frac{\pi}{4}-\theta\right)\right)$
Area 3	$\theta \in \left]\operatorname{atan}\left(\frac{Pitch_{init}/2}{R+Pitch_{init}/2}\right); \frac{\pi}{4}\right]$	$= \sqrt{2} Pitch_{init}.\cos\left(\frac{\pi}{4}-\theta\right)$

initial pitch and shows that these distances mainly depend on the initial pitch value. Introducing $Pitch_{area}(\theta)$ in (Eq. 4), it can be defined $Depth(\theta)$ in relation with angle θ (Eq. 10). Since the reference origin is on the upper surface, the $Depth(\theta)$ is defined negative.

$$Depth(\theta) = -Ke \times \frac{\sqrt{\pi} \times H(Vf) \times B(Vf)}{Pitch_{area}(\theta)} \quad (10)$$

From Eq. 10, for different values of $Pitch_{init}$, $Depth(\theta)$ was plotted on Fig. 8b using $H(Vf) = 0.154$ mm, $B(Vf) = 1.577$ mm et $Ke = 1.1$. These values are derived from the coefficients determined by the rapid calibration procedure (see Sect. 3.1).

Let us study the relative variation in depth. Let $Depth_{init}$ be the depth obtained with a pitch equal to $Pitch_{init}$ (Eq. 11).

$$Depth_{init} = -Ke \times \frac{\sqrt{\pi} \times H(Vf) \times B(Vf)}{Pitch_{\text{init}}} \quad (11)$$

The relative variation in depth is defined by:

$$\Delta Depth(\theta) = \frac{Depth(\theta) - Depth_{init}}{Depth_{init}} = \frac{Pitch_{init}}{Pitch_{area}(\theta)} - 1 \quad (12)$$

By reporting in Eqs. 12, 10 and 11, we obtain, according to the values of $Pitch_{area}(\theta)$ of Table 2, equations of the relative depth variation. Corresponding results are presented in Table 3.

These expressions show that the relative depth variation is independent of $Pitch_{init}$. A single and unique curve (Fig. 9) can thus be plotted to represent the relative depth variation in relation to angle θ.

2.4 Conclusion on change of direction at constant radius

The geometric study of the distance between two consecutive passes with the constant radius R and the use of the simplified model for depth (Eq. 11) allow the following results to be established:

1. The distance between two adjacent toolpaths does not depend on that radius (R) but depends on the initial pitch ($Pitch_{init}$).
2. The relative depth variation is only dependant of angle θ (Table 3 and Fig. 9).
3. The milled depth in a pocket corner can be predicted with a given constant radius by using the initial depth defined by (Eq. 11) and $Pitch_{area}(\theta)$.

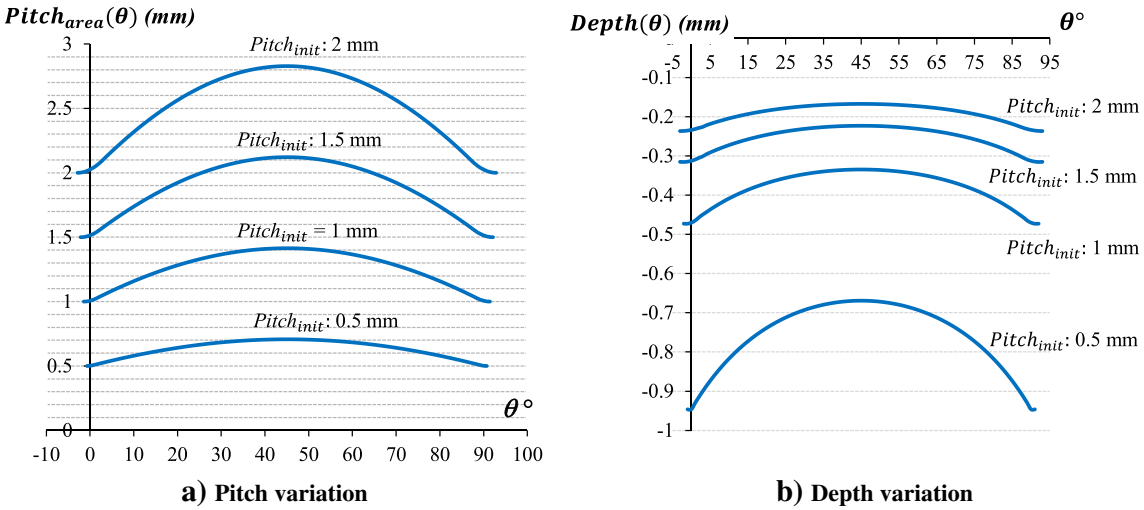

Fig. 8 Pitch and depth variations in constant radius strategy

Table 3 Relative depth variation in the three areas

	Angle (θ)	$\Delta Depth(\theta)$
Area 1	$\theta \cong 0$	$\cong 0$
Area 2	$\theta \in \left]0; \operatorname{atan}\left(\frac{Pitch_{init}/2}{R+Pitch_{init}/2}\right)\right]$	$\cong \frac{2}{1+\sqrt{2}\cos\left(\frac{\pi}{4}-\theta\right)}-1$
Area 3	$\theta \in \left]\operatorname{atan}\left(\frac{Pitch_{init}/2}{R+Pitch_{init}/2}\right); \frac{\pi}{4}\right]$	$\frac{1}{\sqrt{2}\cos\left(\frac{\pi}{4}-\theta\right)}-1$

2.5 Adaptive speed control during change of direction at constant radius

Let Vf_{init} be the traverse speed to obtain a depth $Depth_{init}$ from a pitch $Pitch_{init}$ (Eq. 11). In the circular area, traverse speed is modified to have a constant depth. This leads to:

$$Depth(\theta) = Depth_{init} \tag{13}$$

By reporting Eqs. 2, 10 and 11 in 13, traverse speed modified Vf(θ) is defined by:

$$Vf(\theta) = Vf_{init}\left(\frac{Pitch_{area}(\theta)}{Pitch_{init}}\right)^{\left(\frac{1}{Hv+Bv}\right)} \tag{14}$$

Consider now a pocket whose initial depth is $Depth_{init}$ and a tolerance $\pm T_{Depth}$ (Fig. 10a). On milling of the pocket corner, the depth diminishes and its variation reaches the upper limit $Depth_{init} + T_{Depth}$ for an angular value θ_0. The initial speed is then modified considering a corrected depth $Depth(\theta_0)$ calculated by equation (Eq. 15).

$$Depth(\theta_0) = Depth_{init} - T_{Depth} \tag{15}$$

Using (Eq. 10), the modified traverse speed is:

$$Vf(\theta_0) = \left(\frac{(T_{Depth} - Depth_{init})Pitch_{area}(\theta_0)}{Ke\sqrt{\pi}BoHo}\right)^{\left(\frac{1}{Hv+Bv}\right)} \tag{16}$$

When the tolerance is lower (Fig. 10b), the approach must be iterative and several changes in speed are required. The representation in Fig. 10 assumes instantaneous speed changes.

3 Experimental validation

3.1 Experimental validation of adaptive speed control

The machine configuration is defined by a Flow MACH4-C machine (Fig. 11), a nominal pressure of 100 MPa and an abrasive with grain size 120 mesh and flow 0.34 kg/min. The cutting head is equipped with a nozzle diameter 0.3302 mm and a focusing tube of diameter 1.016 mm and 101.6 mm in length.

The material is Ti6Al4V titanium alloy as previously described. The rapid calibration procedure described in article [15] was applied. Coefficients $Ho = 69.255$, $Hv = -0.935$, $Bo = 1.662$, $Bv = -0.008$ and $Ke = 1.1$ were determined. Based on a pitch equal to $0.6B(Vf)$ as recommended in [15], the traverse speed is 688.3 mm/min to obtain a pocket depth of 0.5 mm (Eq. 4).

Five different milling operations were conducted (Fig. 12):

– Milling with concentric radii (R varying from 0.05 to 20 mm) to check obtaining a flat bottom when the distance between successive trajectories remained constant.

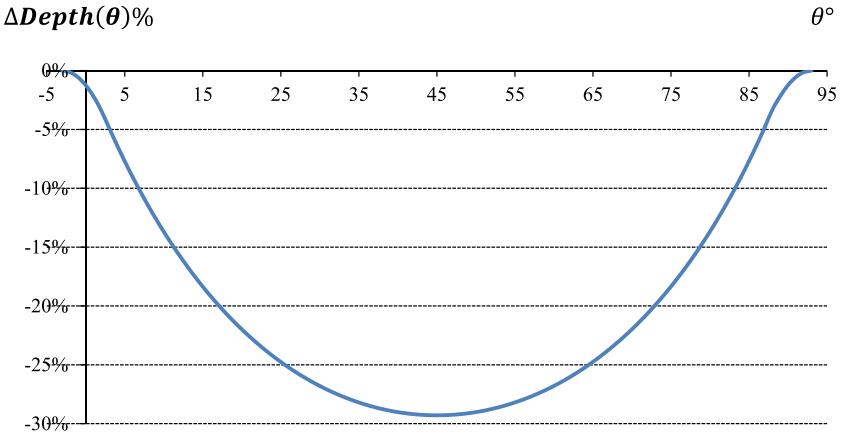

Fig. 9 Relative depth variation for a constant radius strategy

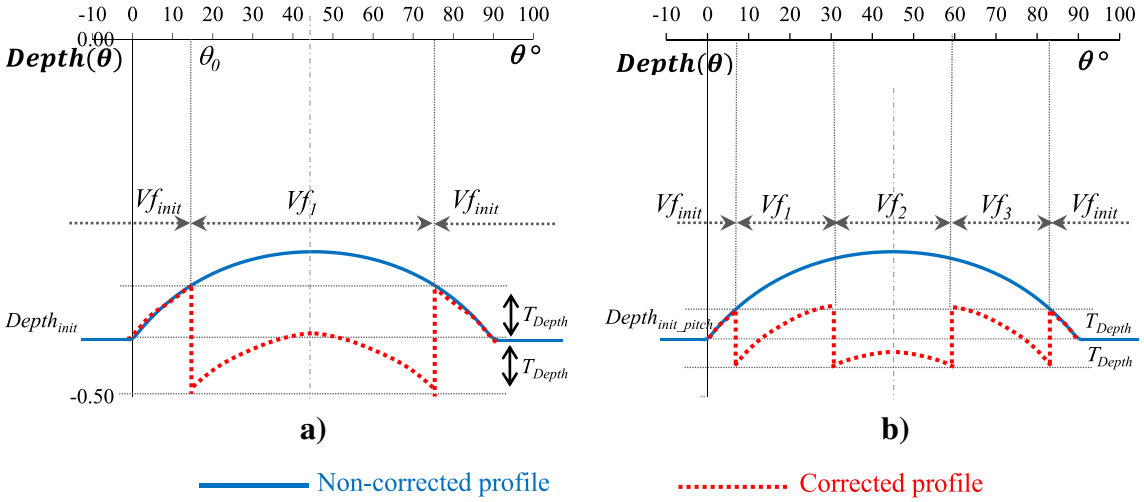

Fig. 10 Correction of the pocket corner depth

– Milling with constant radius $R = 20$ mm to show the speed bump.
– Three milling operations with speed correction for radii $R = 25$ mm, $R = 20$ mm and $R = 15$ mm to validate the method. For these three cases, a tolerance of ± 0.05 mm was considered and four adaptations of the speed were needed to respect that (Fig. 12).

Measurements of the profiles milled were conducted using an Alicona IF profilometer (Fig. 13). This autofocus instrument allows a square zone with 25-mm sides to be mapped taking the coordinates of pixels some micrometres square to within an accuracy of a few micrometres. Precise mappings of the zones measured can be constructed (Fig. 14) by making several acquisitions. To measure a profile, two straight lines are plotted on the surface measured (Fig. 13) and the intersection of their projection over the measured surface is then constructed. This intersection constitutes the profile measured, and its plot can be generated considering the Y and Z coordinates.

3.2 Results and discussion

The results are shown in Fig. 14. A recalibration was made in the Y direction (Fig. 13) to compare the profiles measured whose abscissa is in millimetres and the theoretical profiles whose abscissa is in degrees.

The maximum obtained depth was 0.57 mm (Fig. 14). This is slightly greater than the target depth of 0.5 mm and is the result of a pressure of 110 MPa during the tests instead of the programmed pressure of 100 MPa. The variation comes from the machine that is a cutting machine not provided with a pressure control loop for which the manufacturer chose to increase that parameter to ensure cutting. The modelled profiles were therefore adjusted considering an erosion coefficient Ke of 1.22 instead of 1.1 (Eq. 4). The profiles measured

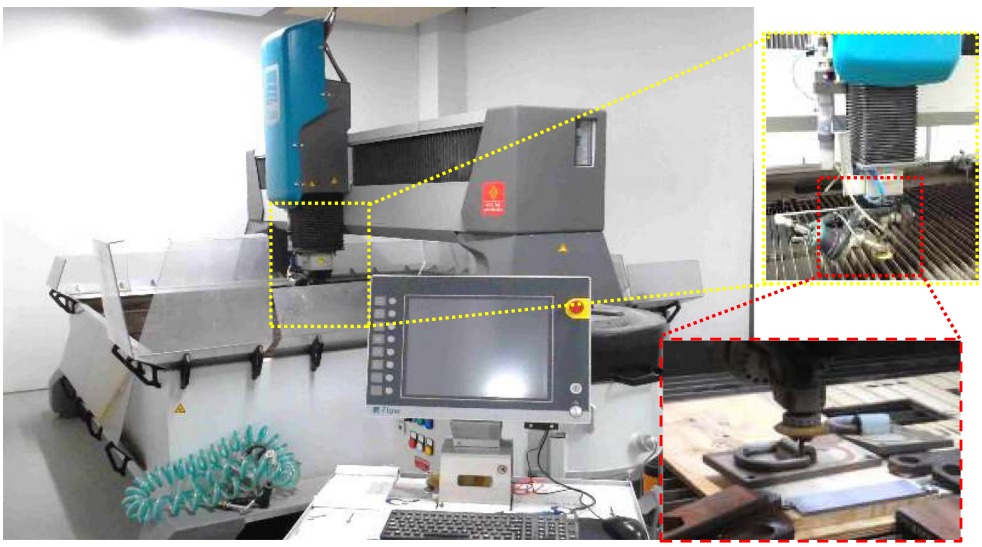

Fig. 11 FLOW MACH4C machine

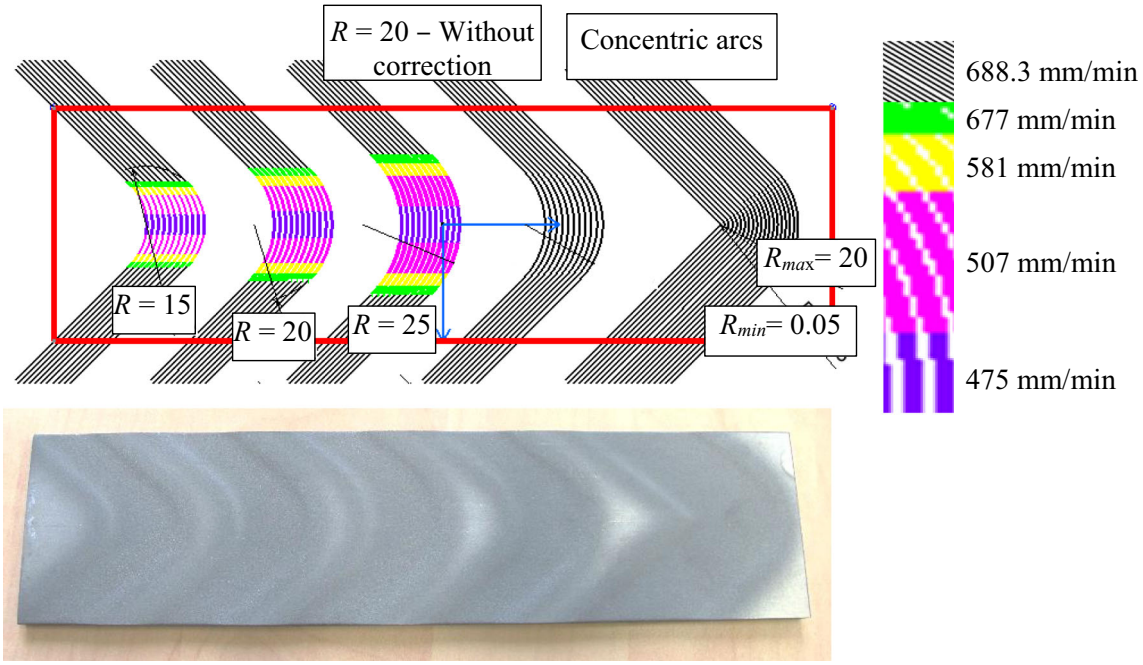

Fig. 12 Ti6Al4V milled

were extremely close to the modelled profiles. This shows, firstly, that the prediction of the initial speed bump defect is accurate and, secondly, that the correction method proposed is effective. The results confirm that the radius *R* does not influence the defect and that the latter is only related to the pitch. The profiles show that the changes in speed are barely perceptible on the milled surface. The *SOD* = 100 mm forms a spot of approximately 7 mm in diameter. Therefore, each point of the surface is milled at least 0.61 s, regardless of the changes in traverse speed. Smoothing effect is thus produced on the surface.

4 Conclusion

The study presented highlights the issue of changes of direction during abrasive waterjet milling of pocket corners. It shows that right-angled changes of direction are not suited to the process as they require a passage through a zero rate that generates an excess depth. It is also shown that concentric arcs alone are not possible since the outer radius is then determined by the scanning pitch and the number of previous passes. This radius cannot then respect a given specification. The paper emphasises the need to mill pocket corners using a constant radius. In this case, a speed bump type defect will appear on the pocket corner bottom. This defect is related to a variable distance between two consecutive toolpaths. This variation in distance leads to a variation in the distribution of the jet's energy that itself leads to a variation in the milled depth. The geometric study of the distance between two passes shows that this variation in distance is not related to the circular arc radius and depends only on the scanning pitch considered. The

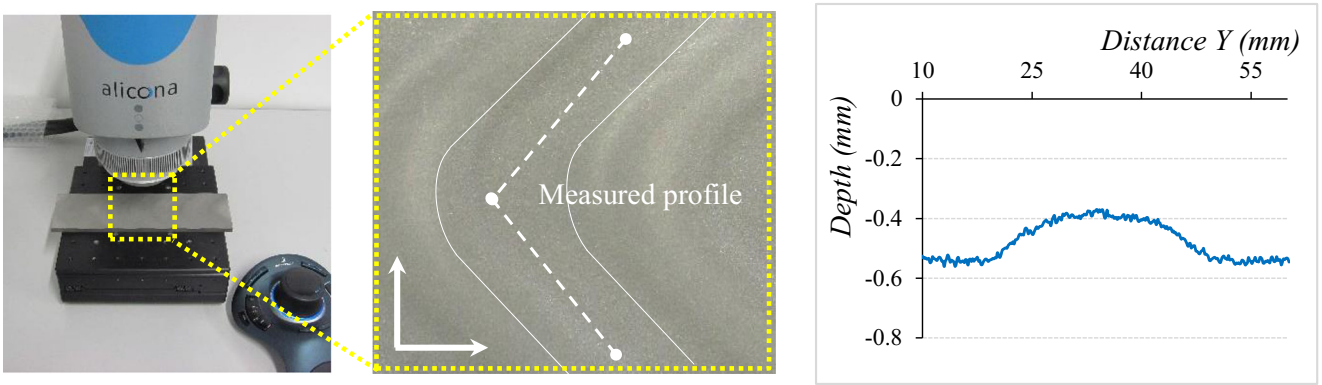

Fig. 13 Measuring a profile

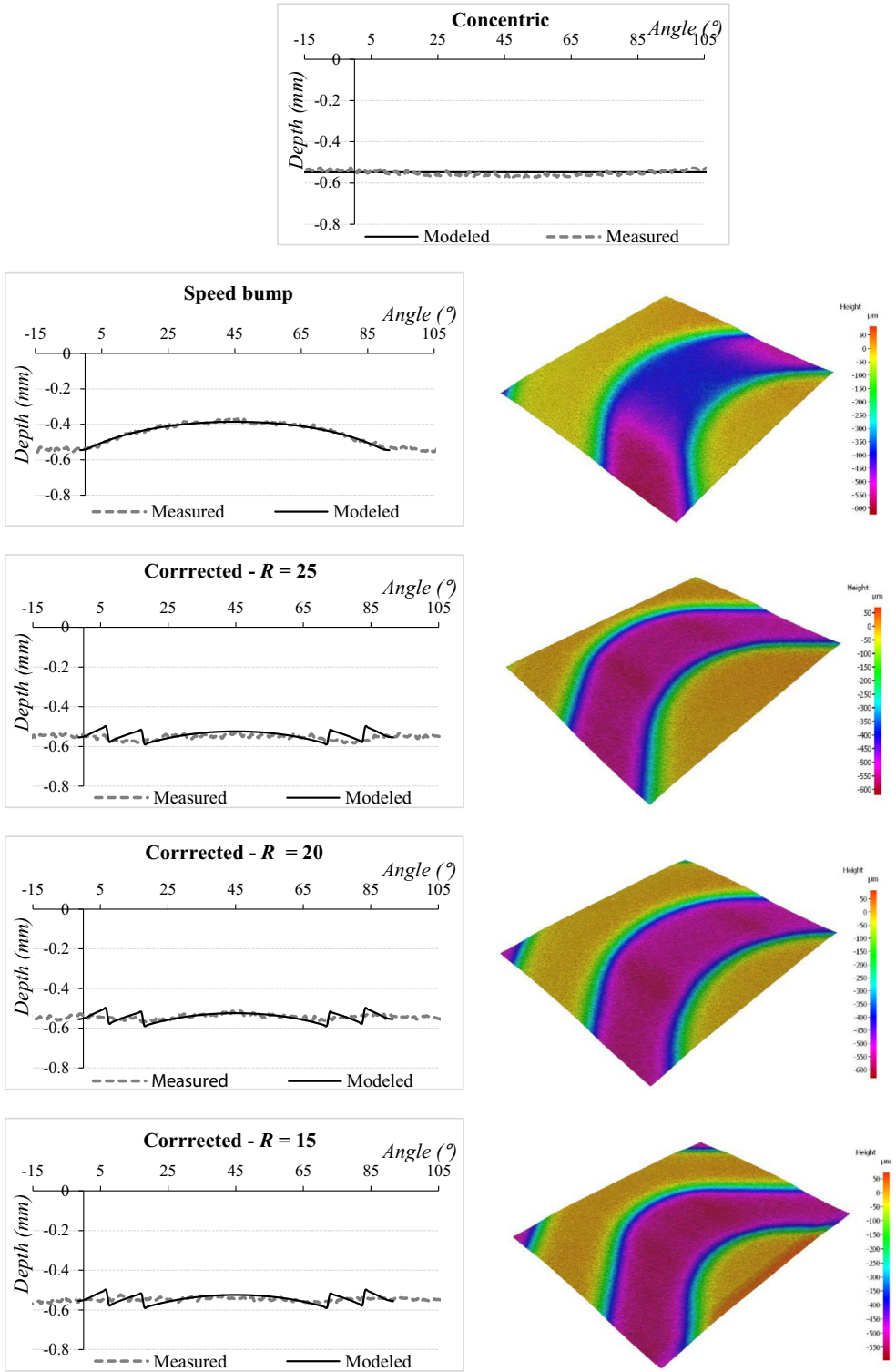

Fig. 14 Modelled and measured profiles

study defines a rational curve to model the variation in depth whatever the pocket corner radius and pitch considered. An adaptive method for speed correction combined with a tolerance on the depth is also adopted. Finally, experimental validation is presented to show the relevance of the geometric approach allowing the initial defect to be predicted. The performance of adaptive control is also validated by tests. The results show that the entire study is coherent and a forthcoming paper will develop a comprehensive milling strategy to mill rectangular pockets consistent with a tolerance on the milled depth.

Appendix

Using Eqs. 5 to 9, the variation between the outer toolpath and inter toolpath for the three areas 1, 2 and 3 can be evaluated (Fig. 7):

1. Area 1: distances in this area, $Pitch_{area1}$, are calculated considering the angle $\theta \in [\theta_1, 0]$ with θ_1 defined by:

$$\theta_1 = atan\left(\frac{-Pitch_{init}/2}{R-Pitch_{init}/2}\right) \tag{17}$$

In this area, segments are always parallel to the X-axis and, from Eqs. 5 and 8, the length of these segments is identified by:

$$Pitch_{area1} = R + Pitch_{init} - \sqrt{R^2 - y^2} \tag{18}$$

Relation between y and θ is given by:

$$\tan(\theta) = \frac{-(Pitch_{init}/2 - y)}{R-Pitch_{init}/2} \tag{19}$$

Replacing y from Eqs. 19 in 18, $Pitch_{area1}$ is obtained by:

$$Pitch_{area1} = R + Pitch_{init} - \sqrt{R^2 - [(R-Pitch_{init}/2)\tan\theta + Pitch_{init}/2]^2} \tag{20}$$

For $\theta = \theta_1$, $Pitch_{area1} = Pitch_{init}$ and for $\theta = 0$, Eq. 20 becomes:

$$Pitch_{area1} = R + Pitch_{init} - \sqrt{R^2 - [Pitch_{init}/2]^2} \tag{21}$$

Considering $Pitch_{init} \ll R$, Eq. 21 can be written:

$$Pitch_{area1} \cong Pitch_{init}\left(1 + 1/\left(8R\right)\right) \cong Pitch_{init} \tag{22}$$

2. Area 2: distances in this area, $Pitch_{area2}$, are calculated considering the angle $\theta \in [0, \theta_2]$ with θ_2 defined by:

$$\theta_2 = \text{atan}\left(\frac{Pitch_{init}/2}{R + Pitch_{init}/2}\right) \tag{23}$$

This angular position θ is linked to $Pitch_{area2}$ by the length:

$$\cos\theta = \frac{R + Pitch_{init}/2}{O_{Cm}A + AB} \tag{24}$$

Considering the triangle $O_{C2}O_{Cm}A$, it can be established:

$$O_{Cm}A^2 - \sqrt{2}Pitch_{init}\cos\left(\frac{3\pi}{4} + \theta\right)O_{Cm}A + \left(\frac{1}{2}Pitch_{init}{}^2 - R^2\right) = 0 \tag{25}$$

Solving Eq. 25, it is possible to calculate $O_{Cm}A$:

$$O_{Cm}A = \frac{-\sqrt{2}Pitch_{init}\cos\left(\frac{\pi}{4} - \theta\right) + \sqrt{4R^2 - 2Pitch_{init}{}^2\sin^2\left(\frac{\pi}{4} - \theta\right)}}{2} \tag{26}$$

As $Pitch_{init} \ll R$, Eq. 26 becomes:

$$O_{Cm}A \cong \frac{-\sqrt{2}Pitch_{init}\cos\left(\frac{\pi}{4} - \theta\right) + 2R}{2} \tag{27}$$

Substituting $O_{Cm}A$ (Eq. 27) into Eq. 24, it is possible to calculate the length:

$$Pitch_{area2} = AB \cong \frac{R(1-\cos\theta) + \frac{Pitch_{init}}{2}\left[1 + \sqrt{2}\cos\theta\cos\left(\frac{\pi}{4} - \theta\right)\right]}{\cos\theta} \tag{28}$$

As $Pitch_{init} \ll R$, the calculated angle θ is small and the length AB can be approximated:

$$Pitch_{area2} \cong \frac{Pitch_{init}}{2}\left(1 + \sqrt{2}\cos\left(\frac{\pi}{4} - \theta\right)\right) \tag{29}$$

3. Area 3: distances in this area, $Pitch_{area3}$, are calculated considering the angle $\theta \in \left[\theta_2, \frac{\pi}{4}\right]$. From Fig. 7, the distances, $Pitch_{area3}$, are defined by:

$$Pitch_{area3} = EF = O_{Cm}F - O_{Cm}E \tag{30}$$

Considering the triangle $O_{C1}O_{Cm}F$, the expression can be established:

$$FO_{Cm}{}^2 + O_{C1}O_{Cm}{}^2 - 2O_{C1}O_{Cm}.FO_{Cm}.\cos\left(\frac{\pi}{4} - \theta\right) = FO_{C1}{}^2 \tag{31}$$

Considering that $O_{C1}O_{Cm} = \frac{\sqrt{2}Pitch_{init}}{2}$ and $FO_{C1} = R$, a new expression is established:

$$FO_{Cm}{}^2 - \sqrt{2}Pitch_{init}.\cos\left(\frac{\pi}{4} - \theta\right).FO_{Cm} + \frac{1}{2}Pitch_{init}{}^2 - R^2 = 0 \tag{32}$$

Similarly, considering triangle $O_{C2}O_{Cm}E$, it can be written:

$$EO_{Cm}{}^2 + \sqrt{2}Pitch_{init}.\cos\left(\frac{\pi}{4}-\theta\right).EO_{Cm} + \frac{1}{2}Pitch_{init}{}^2 - R^2 = 0 \quad (33)$$

Subtracting Eq. 33 from Eq. 32, a simplified expression is established:

$$\left(FO_{Cm}{}^2 - EO_{Cm}{}^2\right) - \sqrt{2}Pitch_{init}.\cos\left(\frac{\pi}{4}-\theta\right).\left(FO_{Cm} + EO_{Cm}\right) = 0 \quad (34)$$

The distance $Pitch_{area3}$ can be calculated by:

$$Pitch_{area3} = EF = FO_{Cm} - EO_{Cm} = \sqrt{2}Pitch_{init}.\cos\left(\frac{\pi}{4}-\theta\right) \quad (35)$$

References

1. Alberdi A, Rivero A, de Lacalle LNL (2011) Experimental study of the slot overlapping and tool path variation effect in abrasive waterjet milling. J Manuf Sci Eng 133(3):034502-1–034502-4
2. Escobar-Palafox G, Gault RS, Ridgway K (2012) Characterisation of abrasive waterjet process for pocket milling in Inconel 718. Procedia CIRP 1:404–408
3. Paul S, Hoogstrate AM, van Luttervelt CA, Kals HJJ (1998) An experimental investigation of rectangular pocket milling with abrasive water jet. J Mater Process Technol 73(1–3):179–188
4. Goutham U, Hasu BS, Chakraverti G, Kanthababu M (2016) Experimental investigation of pocket milling on Inconel 825 using abrasive water jet machining. Int J Curr Eng Technol 6(1):295–302
5. Fowler G, Shipway PH, Pashby IR (2005) Abrasive water-jet controlled depth milling of Ti6Al4V alloy—an investigation of the role of jet–workpiece traverse speed and abrasive grit size on the characteristics of the milled material. J Mater Process Technol 161(3): 407–414
6. Srinivasu DS, Axinte DA, Shipway PH, Folkes J (2009) Influence of kinematic operating parameters on kerf geometry in abrasive waterjet machining of silicon carbide ceramics. Int J Mach Tools Manuf 49(14):1077–1088
7. Alberdi A, Rivero A, López de Lacalle LN, Etxeberria I, Suárez A (2010) Effect of process parameter on the kerf geometry in abrasive water jet milling. Int J Adv Manuf Technol 51(5):467–480
8. Carrascal A, Alberdi A (2010) Evolutionary industrial physical model generation. Proceeding of the International Conference HAIS 2010, San Sebastian, Part I, p 327–334
9. Dittrich M, Dix M, Kuhl M, Palumbo B, Tagliaferri F (2014) Process analysis of water abrasive fine jet structuring of ceramic surfaces via design of experiment. Procedia CIRP 14:442–447
10. Nguyen T, Wang J, Li W (2015) Process models for controlled-depth abrasive waterjet milling of amorphous glasses. Int J Adv Manuf Technol 77(5):1177–1189
11. Boud F, Loo LF, Kinnell PK (2014) The impact of plain waterjet machining on the surface integrity of aluminium 7475. Procedia CIRP 13:382–386
12. Kowsari K, Nouraeia H, Samarehb B, Papini M, Spelt JK (2016) CFD-aided prediction of the shape of abrasive slurry jet micro-machined channels in sintered ceramics. Ceram Int 42(6):7030–7042
13. Tamannaee N, Spelt JK, Papini M (2016) Abrasive slurry jet micro-machining of edges, planar areas and transitional slopes in a talc-filled co-polymer. Precis Eng 43:52–62
14. Anwar S, Axinte DA, Becker AA (2013) Finite element modelling of overlapping abrasive waterjet milled footprints. Wear 303(1–2): 426–436
15. Bui VH, Gilles P, Sultan T, Cohen G, Rubio W (2017) A new cutting depth model with rapid calibration in abrasive water jet machining of titanium alloy. Int J Adv Manuf Technol 93(5–8): 1499–1512
16. Finnie I (1960) Erosion of surface by solid particles. Wear 3(2):87–103
17. Bitter JGA (1963) A study of erosion phenomena—part 2. Wear 6(3):169–190
18. Hashish M (1987) Milling with abrasive-waterjets: a preliminary investigation. In Proceeding of the fourth U.S. waterjet conference, p 1–20
19. Hlaváč LM, Strnadel B, Kaličinský J, Gembalová L (2012) The model of product distortion in AWJ cutting. Int J Adv Manuf Technol 62(1–4):157–166